Extracting Microfacet-based BRDF Parameters from Arbitrary Materials with Power Iterations

Jonathan Dupuy, Eric Heitz, Jean-Claude Iehl, Pierre Poulin, Victor Ostromoukhov

Eurographics Symposium on Rendering 2015
J. Lehtinen and D. Nowrouzezahrai
(Guest Editors)

Volume 34 (2015), Number 4

Extracting Microfacet-based BRDF Parameters from Arbitrary Materials with Power Iterations

Jonathan Dupuy[1,2] Eric Heitz[3] Jean-Claude Iehl[1] Pierre Poulin[2] Victor Ostromoukhov[1] †

[1]LIRIS, Université Lyon 1 [2]LIGUM, Université de Montréal [3]Karlsruhe Institute of Technology

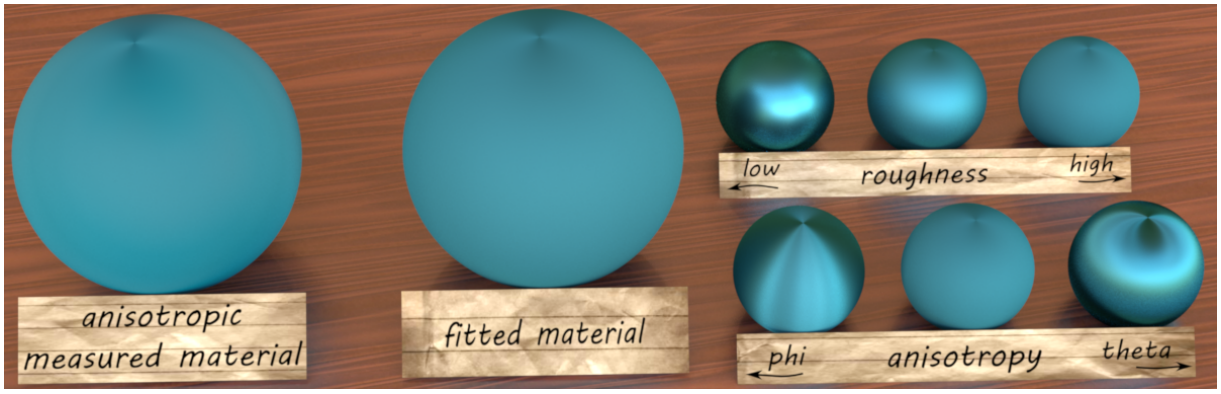

Figure 1: *Given a measured material, our algorithm produces a physically sound microfacet BRDF that closely matches the original appearance, and allows for artistic authoring.*

Abstract

We introduce a novel fitting procedure that takes as input an arbitrary material, possibly anisotropic, and automatically converts it to a microfacet BRDF. Our algorithm is based on the property that the distribution of microfacets may be retrieved by solving an eigenvector problem that is built solely from backscattering samples. We show that the eigenvector associated to the largest eigenvalue is always the only solution to this problem, and compute it using the power iteration method. This approach is straightforward to implement, much faster to compute, and considerably more robust than solutions based on nonlinear optimizations. In addition, we provide simple conversion procedures of our fits into both Beckmann and GGX roughness parameters, and discuss the advantages of microfacet slope space to make our fits editable. We apply our method to measured materials from two large databases that include anisotropic materials, and demonstrate the benefits of spatially varying roughness on texture mapped geometric models.

Categories and Subject Descriptors (according to ACM CCS): I.3.3 [Computer Graphics]: Picture/Image Generation—Antialiasing I.3.7 [Computer Graphics]: Three-Dimensional Graphics and Realism—Color, shading, shadowing, and texture.

† {jdupuy | jciehl | victor.ostromoukhov}@liris.cnrs.fr
eheitz.research@gmail.com
poulin@iro.umontreal.ca

1. Introduction

Material modeling is a fundamental problem in computer graphics. In physically based rendering applications, a material is described by a bidirectional reflectance distribution function, or BRDF for short [NRH*77]. For materials that exhibit specularities ranging from smooth (e.g., plastics) to rough (e.g., metals), the BRDF is typically a derivative of microfacet theory [TS67]. Microfacet BRDFs are driven by physical parameters such as a microfacet normal distribution, roughness, anisotropy, etc. This makes the editing of their parameters to achieve a specific appearance a daunting task. To help with this process, microfacet BRDF fitting may be applied to measured materials.

Existing microfacet-based fitting procedures may be classified in two categories. On the one hand, we find methods that typically introduce a new parametric microfacet normal distribution, and rely on sophisticated optimizations to fit its parameters [NDM05, LKYU12, BSH12]. Although this approach has been used successfully to fit measured materials, current methods suffer from two main problems. First, optimizations are not guaranteed to converge to a valid solution. Second, available parametric models are isotropic and single lobed, which limits the range of materials that they can fit accurately. On the other hand, we find methods that extract an arbitrary microfacet normal distribution into a table [AP07, WZT*08]. While this approach is considerably more general than the ones from the first category, as it naturally supports complex lobes and anisotropy, existing methods are not entirely satisfactory. Indeed, current methods either rely on crude approximations for visibility effects [AP07], or require a complex implementation involving sophisticated optimizations [WZT*08].

In the following sections, we introduce a new tabulation strategy that takes an arbitrary material as input, and extracts a microfacet normal distribution from backscattering configurations, as well as a Fresnel function. Our approach combines the simplicity of the method of Ashikmnin and Premože [AP07], i.e., it is free from sophisticated optimizations, while retaining an accurate model for visibility effects. Specifically, we use the Smith microfacet visibility model [Smi67], which is very popular in the industry [HMD*14]. For real-time rendering applications that require analytic models such as video games, we also provide straightforward routines to convert our fits to Beckmann and GGX microfacet roughness parameters [WMLT07]. Finally, we discuss how implementations may take advantage of microfacet slope space to precompute importance sampling tables that support spatially varying roughness for our fitted materials.

We first recall in Section 2 the fundamentals of microfacet theory and how both roughness and anisotropy can be efficiently controled in slope space. Next, we give an overview of our method in Section 3. We then proceed in Section 4 to show how the problem of recovering a microfacet normal distribution or, equivalently, a microfacet slope distribution, may be transposed into an eigenvector problem. We show that the largest eigenvector is always the solution to this problem, and compute it with the power iteration method. We evaluate the performance of our implementation in Section 5, and discuss conversion into Beckmann and GGX roughness parameters. Finally, we conclude, discuss limitations, and present future perspectives in Section 6.

2. Preliminaries

2.1. Microfacet Theory

Microfacet theory [TS67] is a framework that models the reflectance of rough materials. It describes the BRDF as a global response of a microscopic surface composed of microfacets that act as Fresnel mirrors when radiated by light rays. Under the assumption that single-bounce mirror reflection dominates on the microsurface, the response of the BRDF becomes directly proportional to the probability of finding the visible and illuminated microfacets whose orientations form a mirror-like reflection between given viewing and illumination directions. To express this measure mathematically, we use the coordinate system illustrated in Figure 2. Letting f_r denote the BRDF, $\mathbf{o}$ the viewing direction, $\mathbf{i}$ the illumination direction associated to the infinitesimal solid angle $d\omega_i$, and $\mathbf{h} = (\mathbf{i}+\mathbf{o})/\|\mathbf{i}+\mathbf{o}\|$ the halfway vector, the BRDF takes the analytic form [WMLT07]

$$f_r(\mathbf{i},\mathbf{o}) = \frac{F(\theta_d)\,D(\mathbf{h})\,G(\mathbf{i},\mathbf{o})}{4\cos\theta_i\cos\theta_o}. \tag{1}$$

The angle $\theta_d = \arccos(\mathbf{i}\cdot\mathbf{h}) \in [0,\pi/2]$ is known as the difference angle in the BRDF parameterization of Rusinkiewicz [Rus98], and we follow standard computer graphics notations for the various terms: $F \in [0,1]$ is the

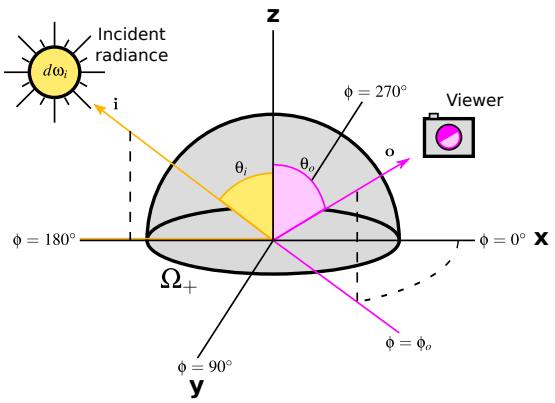

Figure 2: *Coordinate system and relevant quantities:* $\mathbf{i}$*, light source Cartesian unit vector associated to an infinitesimal solid angle* $d\omega_i$*;* $\mathbf{o}$*, viewer Cartesian unit vector;* θ_k $(k = i,o)$*, elevation angle of unit vector* $\mathbf{k} = (\sin\theta_k\cos\phi_k, \sin\theta_k\sin\phi_k, \cos\theta_k)^t$.

microfacet Fresnel term, $D \geq 0$ the microfacet normal distribution function (NDF) of the microsurface, and $G \in [0,1]$ the geometric attenuation factor (GAF) of the microsurface due to masking and shadowing effects.

In current state-of-the-art models, the GAF is given by the correlated bistatic Smith shadowing function [HMD*14]. This model ensures consistency between the projected area of microfacets and the cosine law with respect to directions $\mathbf{o}$ and $\mathbf{i}$ [Hei14]; it may be written as

$$G(\mathbf{i},\mathbf{o}) = \frac{G_1(\mathbf{i})\,G_1(\mathbf{o})}{G_1(\mathbf{i}) + G_1(\mathbf{o}) - G_1(\mathbf{i})\,G_1(\mathbf{o})}, \tag{2}$$

where $G_1 \in [0,1]$ denotes the Smith monostatic shadowing function [Smi67, Hei14]

$$G_1(\mathbf{k}) = \frac{\cos\theta_k}{\int_{\Omega_+} \mathbf{kh}\,D(\mathbf{h})\,d\omega_h}. \tag{3}$$

Note that we use the notation $\mathbf{kh}$ to express a clamped dot product, i.e., $\mathbf{kh} = \max(0, \mathbf{k}\cdot\mathbf{h})$.

2.2. Microfacet Slopes

As is made particularly apparent in Equations (1) and (3), the microfacet NDF plays a major role in the construction of a microfacet BRDF. The microfacet NDF is a directional distribution defined on the hemisphere, and is normalized such that its projection onto the tangent plane has unit area [WMLT07], i.e.,

$$\int_{\Omega_+} D(\mathbf{h})\cos\theta_h\,d\omega_h = 1. \tag{4}$$

A directional distribution is not straightforward to manipulate or design. In contrast to normals, slopes are much easier to study, as they live in the $\mathbb{R}^2$ plane. In the Ω_+ set, normals and slopes are linked through the bijection

$$\tilde{\mathbf{h}} = \begin{bmatrix} -\tan\theta_h\cos\phi_h = \tilde{x}_k \\ -\tan\theta_h\sin\phi_h = \tilde{y}_k \end{bmatrix}, \quad \tilde{\mathbf{h}} \in \mathbb{R}^2, \tag{5}$$

whose inverse is

$$\mathbf{h} = \frac{1}{\sqrt{\tilde{x}_h^2 + \tilde{y}_h^2 + 1}} \begin{bmatrix} -\tilde{x}_h \\ -\tilde{y}_h \\ 1 \end{bmatrix}, \quad \mathbf{h} \in \Omega_+. \tag{6}$$

From this relation, we may define a microfacet NDF from a bivariate slope probability distribution function $P \geq 0$ such that

$$D(\mathbf{h}) = P(\tilde{\mathbf{h}})\,\sec^4\theta_h. \tag{7}$$

The secant term is the Jacobian that converts the measure of microfacet slope probability into a microfacet normal distribution [Hei14]. As long as P is a normalized PDF, i.e.,

$$\int_{\mathbb{R}^2} P(\tilde{\mathbf{h}})\,d\tilde{\mathbf{h}} = 1, \tag{8}$$

Equation (4) holds. The introduction of such a PDF is particularly convenient for importance sampling, since the simulation of such variates simply requires the computation of two quantile functions, as we show in Appendix A.

2.3. Microfacet Roughness

Another benefit of working with slopes is that, in slope space, control over roughness gets a precise physical interpretation: it is inversely proportional to horizontal scaling transformations. This is intuitive: the more the slopes are stretched, the smoother the surface. Conversely, the more the slopes are contracted, the rougher the surface. If we let $\alpha_x > 0$ and $\alpha_y > 0$ respectively denote microfacet roughness in the x and y directions, then we may define a microfacet NDF with explicit control over roughness and anisotropy as

$$D(\mathbf{h};\alpha_x,\alpha_y) = P\left(\frac{\tilde{x}_h}{\alpha_x}, \frac{\tilde{y}_h}{\alpha_y}\right)\frac{\sec^4\theta_h}{\alpha_x\alpha_y}. \tag{9}$$

Note that this expression of D still satisfies Equation (4). Furthermore, if we have an importance sampling strategy for P, then we can easily adapt it to roughness by scaling the variate by α_x and α_y. We refer to this property as roughness invariance. It may be shown that G_1 is also roughness invariant [Hei14].

3. Overview

With the state-of-the-art microfacet theory at hand, we may now move on to the problem of retrieving a microfacet BRDF from an input material. Note that, in the fitting scheme that we introduce next, we focus on retrieving P rather than D. While this approach does not impact fitting performance, i.e., retrieving either P or D with our method will produce the same fits, tabulating P directly allows us to perform offset and interpolated table lookups in our implementation, which we exploit to perform roughness manipulation. We then precompute G_1 and the quantile functions used for importance sampling into tables.

We also differ from previous fitting methods in two additional aspects. First, our fitting scheme does not attempt to retrieve a Lambertian term; it extracts microfacet terms exclusively. As such, we can not recover mixtures of both models. Second, we do not build a microfacet distribution for each color channel. Originally, this approach was motivated by our desire to enforce physical soundness: microfacet BRDFs are based on the geometric optics approximation, and creating per wavelength microscopic surfaces makes no sense. In practice, we noted that our fits had sufficient quality with this restriction, and that fitting errors were due to limitations of the microfacet theory itself. Nonetheless, nothing prevents our fitting to apply to each color channel.

Finally, we also mention that if P is isotropic, then we can perform importance sampling according to the distribution of visible slopes [HD14]. This strategy works for any isotropic material.

4. Microfacet Extraction

4.1. Backscattering Configurations

In order to retrieve a microfacet slope distribution from an input material, we are going to use a simplified form of Equation (1). Specifically, we focus on backscattering configurations, which reduces the dimensionality of the BRDF, and simplifies the Fresnel term to a constant. Indeed, in such configurations, we have $\mathbf{i} = \mathbf{o} = \mathbf{h}$, as well as $\theta_d = 0$; for convenience, we write $F_0 = F(0)$. Equation (1) predicts that the BRDF takes the form

$$f_r(\mathbf{o},\mathbf{o}) = \frac{F_0\, D(\mathbf{o})\, G(\mathbf{o},\mathbf{o})}{4\cos^2\theta_o}. \tag{10}$$

However, this is not entirely accurate because the GAF, i.e., G, overestimates shadowing effects. When $\mathbf{i} = \mathbf{o}$, shadowing and masking are fully correlated, and the GAF should degenerate into the monostatic form [Hei14]

$$G(\mathbf{o},\mathbf{o}) = G_1(\mathbf{o}). \tag{11}$$

The accurate form of the GAF term leads to the microfacet backscattering equation

$$f_r(\mathbf{o},\mathbf{o}) = \frac{F_0\, D(\mathbf{o})\, G_1(\mathbf{o})}{4\cos^2\theta_o}. \tag{12}$$

With this equation at hand, we may now proceed to the extraction of a microfacet slope distribution, i.e., P, given an input material f_r. Note that the inability of Equation (2) to degenerate into Equation (11) is known as the hotspot problem, and remains an open problem. In practice, we use Equation (11) for fitting purposes and Equation (2) for rendering. Our results thus slightly overestimate occlusion effects in hotspot configurations by the factor $1/(2-G_1) \in [0.5, 1]$.

4.2. Eigensystem Construction

In our microfacet BRDF fitting problem, we are given an input material f_r and asked to extract a microfacet Fresnel term and a microfacet slope distribution. As a first step towards this direction, we swap the product $F_0\, D$ and f_r to the other side of the equality in the microfacet backscattering equation, i.e., Equation (12). This yields

$$F_0\, D(\mathbf{o}) = \frac{4 f_r(\mathbf{o},\mathbf{o})\cos^2\theta_o}{G_1(\mathbf{o})}. \tag{13}$$

Next, by replacing D and G_1 in Equation (13) by their respective definitions, i.e., Equation (7) and Equation (3) respectively, we get an equation for the microfacet slope PDF

$$F_0\, P(\tilde{\mathbf{o}}) = \int_{\Omega_+} K(\mathbf{o},\mathbf{h})\, P(\tilde{\mathbf{h}})\, d\omega_h, \tag{14}$$

where

$$K(\mathbf{o},\mathbf{h}) = 4 f_r(\mathbf{o},\mathbf{o})\, \cos^5\theta_o\, \mathbf{oh}\, \sec^4\theta_h. \tag{15}$$

Equation (14) is not trivial to solve: in the mathematics literature, it belongs to the family of multivariate Fredholm equations of the second kind with kernel K [PM12]. In our case, the form of the kernel is not known in advance due to the input material f_r, so we solve this equation numerically by discretizing Equation (14) with a quadrature rule. Letting w_j denote the j-th quadrature rule weight and $i = 1, \cdots, N$, we obtain the new relation

$$F_0\, P(\tilde{\mathbf{o}}_i) = \sum_{j=1}^{N} w_j\, K(\mathbf{o}_i,\mathbf{h}_j)\, P(\tilde{\mathbf{h}}_j), \tag{16}$$

where $\tilde{\mathbf{o}}_1 = \tilde{\mathbf{h}}_1, \cdots, \tilde{\mathbf{o}}_N = \tilde{\mathbf{h}}_N$ are the (slope) quadrature points, located in $\mathbb{R}^2$. Now, letting $\mathbf{p}$ denote the discretized PDF vector $\mathbf{p} = (P(\tilde{\mathbf{o}}_1), \cdots, P(\tilde{\mathbf{o}}_N))^t$ and $\mathbf{K}$ the matrix

$$\mathbf{K} = \begin{bmatrix} w_1 K(\mathbf{o}_1,\mathbf{h}_1) & \cdots & w_N K(\mathbf{o}_1,\mathbf{h}_N) \\ \vdots & \ddots & \vdots \\ w_1 K(\mathbf{o}_N,\mathbf{h}_1) & \cdots & w_N K(\mathbf{o}_N,\mathbf{h}_N) \end{bmatrix}. \tag{17}$$

Equation (16) rewrites as the eigenvalue problem

$$F_0\, \mathbf{p} = \mathbf{K} \cdot \mathbf{p}. \tag{18}$$

This result shows that the problem of retrieving a microfacet slope PDF given an input material f_r translates into finding an eigenvector $\mathbf{p}$ whose components are all nonnegative.

4.3. Resolution via Power Iterations

Since the entries of the matrix $\mathbf{K}$ are all nonnegative, the Perron-Frobenius theorem [Per07, Fro12] states that it always has a unique eigenvector $\mathbf{p}$ whose values are all nonnegative. It is thus a valid solution for the microfacet slope distribution P. By solving Equation (18), we therefore have the **guaranteed** ability to compute a valid microfacet slope PDF from an input material. Furthermore, the theorem states that this eigenvector is associated to the largest eigenvalue of the matrix. As such, we can compute it straightforwardly with the power iteration method.

The power iteration method is based on the property that the eigenvector associated to the largest eigenvalue of a matrix emerges after successive multiplications with a vector. In our implementation, we initialize $\mathbf{p} = (1, \cdots, 1)^t$, and successively multiply it by $\mathbf{K}$. In practice, we use only four successive multiplications, which has turned out to be sufficient for all our test cases. Once the vector has been determined, we build a continuous PDF by linearly interpolating the values of $\mathbf{p}$, and normalize it to satisfy Equation (8). We store the result in a table, which completes the extraction of P. Algorithm 1 provides pseudocode for our method.

With the extraction process of P complete, we can now evaluate the microfacet NDF, i.e., D, extracted from the input material thanks to Equation (7). It follows from Equation (3) that we can also compute the Smith term G_1. At this point, we can already create a fully functional microfacet BRDF whose microfacets act as "ideal" mirrors, i.e.,

$$f_{r,id}(\mathbf{i},\mathbf{o}) = \frac{D(\mathbf{h})\, G(\mathbf{i},\mathbf{o})}{4\cos\theta_i \cos\theta_o}. \tag{19}$$

Algorithm 1 Extract P

```
function EXTRACT_P(f_r, N)
    for each i, j ∈ [1, N] do                ▷ Build kernel matrix
        K_{i,j} ← w_j 4 f_r(o_i, o_i) cos^5 θ_{o_i} o_i h_j sec^4 θ_{h_j}
    end for
    p ← (1, ··· , 1)^t
    for 0 ≤ i < M do                         ▷ Power iterations (we set M = 4)
        p ← K · p
    end for
    P ← normalize(p)
end function
```

Note that this equation is a special case of Equation (1), where $F(\theta_d) = 1$ for any θ_d. We can thus turn to the problem of retrieving the microfacet Fresnel term in order to complete the fitting process.

4.4. Fresnel Extraction

In order to extract the Fresnel term, we compute for each color channel the average ratio between the input material and Equation (19) over all possible θ_d configurations, i.e.,

$$F(\theta_d) = \mathbb{E}\left[\frac{f_r(\mathbf{i},\mathbf{o})}{f_{r,id}(\mathbf{i},\mathbf{o})} \,|\, \mathbf{ih} = \cos\theta_d\right], \tag{20}$$

where we use the notation $\mathbb{E}[x|y]$ to denote the expectation of variable x over the domain that satisfies condition y. Algorithm 2 provides pseudocode for our method.

Algorithm 2 Extract F

```
function EXTRACT_F(f_r, f_{r,id})
    for θ_d ∈ [0, π/2] do
        F(θ_d) ← 0
        N ← 0
        for φ_d, φ_h ∈ [0, 2π], θ_h ∈ [0, π/2] do
            i ← from_half_diff(h, d)
            o ← reflect(i, h)
            F(θ_d) ← F(θ_d) + f_r(i, o)/f_{r,id}(i, o)
            N ← N + 1
        end for
        F(θ_d) ← F(θ_d)/N
    end for
end function
```

The main advantage of our approach is that it is fully automatic. It is very accurate when the behavior of the input material accords to microfacet theory, i.e., when f_r is roughly equal to Equation (1). When this condition does not hold, our algorithm will propagate the fitting errors into the Fresnel term. Such situations will arise for, e.g., materials with directionally dependent albedo such as certain fabrics or car paints. In such cases, the extracted behavior of F differs significantly from what is predicted by the Fresnel law, and the term should be regarded as a residual function instead of an actual Fresnel function.

4.5. Optimization: Eigensystem Construction for Isotropic Materials

Although our fitting process is already complete, we introduce here an optimization for the extraction of P that works for isotropic materials. If the input material is isotropic, then the microfacet NDF, i.e., D, depends only on the elevation angle θ_h. It follows from Equation (7) that the microfacet slope PDF is also isotropic, which implies that it may be expressed as a 1D radial function

$$P(\tilde{\mathbf{h}}) = g(\theta_h). \tag{21}$$

In such cases, the problem of retrieving the 2D function P, i.e., Equation (14), simplifies to that of finding the 1D function g. This problem also translates into a (univariate) Fredholm equation of the second kind

$$F_0\, g(\theta_o) = \int_0^{\pi/2} K'(\theta_o,\theta_h)\, g(\theta_h)\, d\theta_h, \tag{22}$$

with kernel K'

$$K'(\theta_o,\theta_h) = \int_0^{2\pi} K(\mathbf{o},\mathbf{h})\, \sin\theta_h\, d\phi_h. \tag{23}$$

We provide the derivations that lead to this particular result in Appendix B. Note that the choice of the azimuthal angle ϕ_o to fully define $\mathbf{o}$ is arbitrary in Equation (23). As for the general case, Equation (22) may be expressed as an eigenvalue problem of the form

$$F_0\, \mathbf{p}' = \mathbf{K}' \cdot \mathbf{p}', \tag{24}$$

where $\mathbf{p}' = (g(\theta_{o_1}), \cdots, g(\theta_{o_N}))^t$. Since the entries of the matrix $\mathbf{K}'$ are also nonnegative, we can also solve Equation (24) with the power iteration method. In practice, we also use four successive multiplications to recover the solution $\mathbf{p}'$. Algorithm 3 provides pseudocode for this specialized method.

Algorithm 3 Extract Isotropic P

```
function EXTRACT_P_ISOTROPIC(f_r, N)
    φ_o ← 0                                  ▷ The choice is arbitrary here
    for each i, j ∈ [1, N] do                ▷ Build kernel matrix
        K'_{i,j} ← ∫_0^{2π} w_j K(o_i, h_j) sin θ_{h_j} dφ_h
    end for
    p' ← (1, ··· , 1)^t
    for 0 ≤ i < M do                         ▷ Power iterations (we set M = 4)
        p' ← K' · p'
    end for
    P ← normalize(p')
end function
```

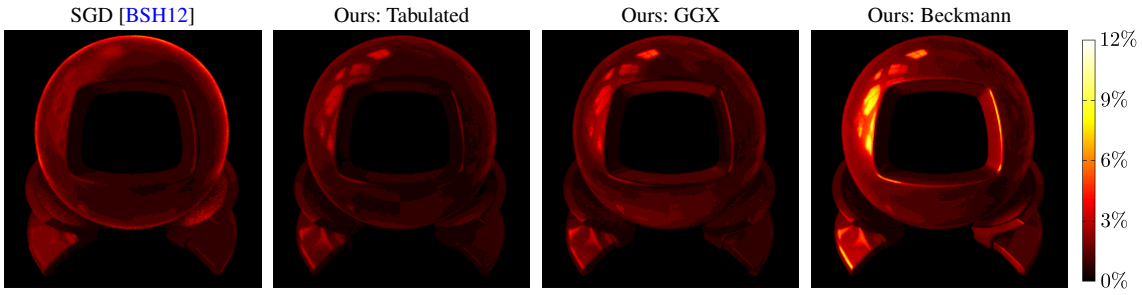

Figure 3: *Mean delta-E difference image on the entire MERL database [MPBM03].*

5. Implementation and Results

5.1. Precomputations

In our implementation, we rely exclusively on rectangle quadrature rules to compute our integrals. This includes the microfacet slope PDF, i.e., $w_1 = \cdots = w_N = 1/N$. We store one RGB table for the microfacet Fresnel, and three scalar-valued 1D (resp. 2D) tables for P, G_1, and the quantile function for isotropic (resp. anisotropic) materials. The dimensions of the tables depend on the number of samples we evaluate from the material in the elevation and azimuthal directions. In the isotropic configuration, the number of samples is equal to N. In this case, our representation stores (including Fresnel and the other tables) $3N + 3N = 6N$ scalar values. In the anisotropic configuration, the number of samples is equal to $N = N_\theta \times N_\phi$, where N_θ and N_ϕ respectively denote the number of elevation and azimuthal samples used to evaluate the reflectance of the input material. In this case, our representation stores (including Fresnel and the other tables) $3N_\theta \times (1 + N_\phi)$ scalar values.

5.2. Online Computations

We implemented BSDF plugins in the Mitsuba renderer [Jak10] to use our microfacet model. Our plugins implement the functions *eval* and *sampling*, which are called by Mitsuba's Monte Carlo integrator. The *eval* function evaluates Equation (1) using the precomputed tables for P, G_1, and F (we get D from P with Equation (7)). The *sample* function calls the precomputed quantile functions Q_1 and Q_2 as explained in Appendix A. Because our tables are roughness invariant, we produce a wide variety of roughness effects on the fly by scaling the lookup parameters by α_x and α_y.

5.3. Experiments

Unit Testing We validated our microfacet slope PDF extraction by testing our algorithms against an analytic model of Equation (12) based on a Beckmann distribution [WMLT07] with varying roughness. Table 1 shows the maximum relative errors we measured during our experiment in the isotropic case, using $N = 360$. As can be seen from the reported numbers, the error is small (less than 1%). We attribute this error to the quadrature rules that we use to solve integral Equations (14) and (22), and consider it as the minimum error produced by our algorithms. The anisotropic case produces the same amount of relative error.

α	0.01	0.02	0.05	0.15
δ_{max}	0.03	0.004	0.002	0.0005

Table 1: *Maximum relative error in backscattering between Beckmann BRDFs with varying roughness and their respective fits computed with our algorithm.*

Fitting Isotropic Materials We proceeded to a fitting comparison against the state-of-the-art parametric model, referred hereafter as SGD, of Bagher et al. [BSH12] using the MERL material database of Matusik et al. [MPBM03]. To compute our fits, we initialized our algorithm with $N = 90$ and made sure that the entire backscattering data was sampled only once. At 32-bit floating-point precision, each of our fits requires 2.1 KB of memory. We provide the exhaustive tests in our supplemental document, which also includes more detailed numerical analysis as well as delta-E difference images. Figure 6 shows some comparative renderings of both methods as well as with the ABC microfacet model [LKYU12] against the reference for a few materials, using 512 samples per pixel. Notice that for the *two-layer-gold* and *changing-paint1* materials, the SGD fitting optimization failed and resulted in flawed images. This example emphasizes one of the strengths of our fitting method over optimization techniques, since, as we showed in the previous section, our fits can not result in such failures. Note that these materials were not the only ones affected by this issue in the database. In general, we believe our method is qualitatively superior to SGD and on par with ABC for metallic materials. Differences with SGD and ABC are most visible in Figure 6 at grazing angles. For most other materials in our supplemental document, our fits are either on par or slightly below the SGD model. While our observation is mainly qualitative, it is also in agreement with the average delta-E difference image of our supplemental document, which is illustrated in Figure 3.

Worse Isotropic Fitting For certain isotropic materials of the MERL database, we noticed that our method could produce fits that were qualitatively less satisfying than previous work. Figure 6 carries a few such materials, which can also be found in our supplemental document. In this particular figure, our fit of the *alumina-oxide* material is worse that those of the ABC and SGD models. We see two reasons why our method would produce less satisfying fits. The first reason is due to the input material itself: since our method extracts the microfacet NDF from backscattering data exclusively, it is highly sensitive to the quality of such configurations. Thus, if backscattering is poorly acquired, then our method will fail at reproducing the input faithfully. Such scenarios are plausible for the *alumina-oxide* material of Figure 6, as our fit results in altered highlights (our fit appears too matte). The second reason is due to our BRDF model: our model is based on a microfacet BRDF model alone and, as such, is limited to material behaviors that are close to what is predicted by the equations. Layered and/or composite materials (e.g., *alumina-oxide* in Figure 6) as well as strong Lambertian component (e.g., some paints and acrylics), tend to be qualitatively less satisfying than the SGD fits in our supplemental document. For isotropic materials with poor backscattering data and/or strong Lambertian components, fitting methods based on optimizations [NDM05, LKYU12, BSH12, WZT*08] should also perform better than our method in general. As for layered and color changing materials (e.g., *changing-paint1* in Figure 6), they remain a challenging open problem.

Fitting Anisotropic Materials Our method also supports anisotropic materials. To review its performance, we tested some highly anisotropic materials from the recent database of Filip and Vavra [FV14]. To compute our fits, we initialized our algorithm with $\theta_N = 90$ and $\phi_N = 90$. At 32-bit floating-point precision, each of our fits requires 6 KB of memory. Our results were computed using 512 samples per pixel and are illustrated in Figure 7. For each material, the lobe of the BRDF (and hence the microfacet NDF) is captured accurately. Note however that our fit of the *fabric106* material failed at reproducing the directionally dependent albedo exhibited by the reference.

5.4. Computational Performance

Speed Our fitting algorithms are very fast: it takes us less than 1 second to fit an isotropic material from the MERL database of Matusik et al. [MPBM03], and less than 20 seconds for an anisotropic material of Filip and Vavra [FV14]. Naturally, fitting performance depends on the resolution of the tables, i.e., on N. We measured the impact of such a factor for both isotropic and anisotropic algorithms. Results are plotted in Figure 5, where the timings include the computations of the slope PDF, the Smith term, the quantile functions, and the Fresnel term on an Intel 2.4GHz Core i5 CPU.

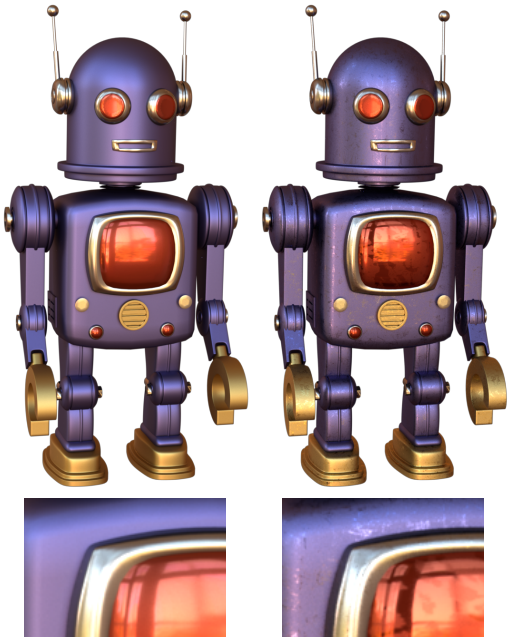

(a) (b)

Figure 4: *Multiple material design on a production asset. (a) Measured BRDFs. (b) Our fitted microfacet BRDFs controled by a roughness texture map. Model courtesy of LAGOA.*

We believe such timings make our method much faster than previous work.

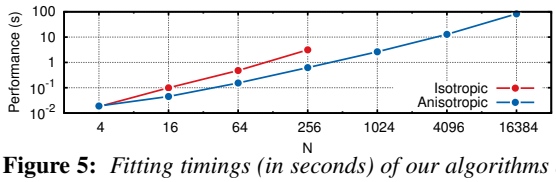

Figure 5: *Fitting timings (in seconds) of our algorithms as a function of the number of input material evaluations.*

Memory Because our representation is roughness invariant, it allows us to create a multitude of materials at constant memory cost. As an example, we rendered the scenes illustrated in Figures 1 and 4 using 512 samples per pixel and a few KB of memory. Such rendering configurations are only possible with slope space tables. Otherwise, the per-pixel sampling rate and/or memory consumption to store importance sampling tables should be increased. For roughness mapped models such as ones shown in Figure 4, where the number of different materials is very high, such approaches would have been particularly impractical. Alongside analytic microfacet BRDF models, we believe our tabulation strategy is the first to support such complex configurations trivially.

Conversion to Analytic BRDFs Although our memory footprint is constant per fitted material, some applications

might not be able to afford the storage of precomputed tables. This is typically the case in real-time rendering contexts, where analytic microfacet BRDF models such as the GGX or Beckmann models are a necessity. In Appendix C, we show that our tabulated microfacet slope PDF can be converted straightforwardly to either GGX or Beckmann roughness parameters using slope moments. With such analytic microfacet models, only the Fresnel table needs to be stored. In order to quantify the loss in fitting quality compared to our tabulated representation, we placed some renderings obtained with the analytic models next to our tabulated fits in Figure 6. We noticed that the GGX model performs generally better than the Beckmann model (see also Figure 3), which is in agreement with previous observations [TR75, WMLT07, Bur12]. Note that we also incorporated the analytic models in our detailed fitting analysis provided in our supplemental document.

6. Conclusion

We introduced a novel method to fit a microfacet BRDF model to an input material. Compared to previous approaches, our method is considerably faster, more robust, and more general. By working in microfacet slope space, we also provide simple and effective control over roughness. We implemented our algorithms in a C++ library that is available on GitHub[†]. Our code allows one to reproduce all our fitting results. We hope this will encourage more research in the direction of fitting physically based materials, as there are still remaining challenges to be undertaken. In particular, the way we extract the Fresnel term needs to be improved. We also believe that our method could be successfully applied to bidirectional transmission distribution functions, as well as spatially varying BRDFs.

Acknowledgements

We thank Thiago Da Costa and Arno Zinke for providing us with the LAGOA robot asset, Brent Burley for useful discussions regarding BRDF authoring in production contexts, and Laurent Pujo-Menjouet and Ionel Ciuperca for their input on integral equations. This research was partly funded by GRAND and the ANR AMCQMCSCGA.

References

[AP07] ASHIKHMIN M., PREMOŽE S.: Distribution-based BRDFs. *Technical Report, University of Utah* (2007). 2

[BSH12] BAGHER M. M., SOLER C., HOLZSCHUCH N.: Accurate fitting of measured reflectances using a shifted gamma micro-facet distribution. *Comput. Graph. Forum 31*, 4 (2012), 1509–1518. 2, 6, 7, 10

[Bur12] BURLEY B.: Physically-based shading at Disney. In *SIGGRAPH 2012 Courses: Practical physically-based shading in film and game production* (2012). 8

[DHI*13] DUPUY J., HEITZ E., IEHL J.-C., POULIN P., NEYRET F., OSTROMOUKHOV V.: Linear efficient antialiased displacement and reflectance mapping. *ACM Trans. Graph. 32*, 6 (Nov. 2013), 211:1–11. 9

[Fro12] FROBENIUS G.: Über matrizen aus nicht negativen elementen, s. *B. Preuss. Akad. Wiss. Berlin* (1912), 456–477. 4

[FV14] FILIP J., VAVRA R.: Template-based sampling of anisotropic BRDFs. *Comput. Graph. Forum (Pacific Graphics) 33*, 7 (2014), 91–99. 7, 10

[HD14] HEITZ E., D'EON E.: Importance sampling microfacet-based BSDFs using the distribution of visible normals. In *Proc. Eurographics Symposium on Rendering* (2014), EGSR, pp. 103–112. 3

[Hei14] HEITZ E.: Understanding the masking-shadowing function in microfacet-based BRDFs. *Journal of Computer Graphics Techniques (JCGT) 3*, 2 (2014), 32–91. 3, 4, 9

[HMD*14] HILL S., MCAULEY S., DUPUY J., GOTANDA Y., HEITZ E., HOFFMAN N., LAGARDE S., LANGLANDS A., MEGIBBEN I., RAYANI F., DE ROUSIERS C.: Physically based shading in theory and practice. In *SIGGRAPH Courses* (2014), ACM, pp. 23:1–8. 2, 3

[Jak10] JAKOB W.: Mitsuba renderer, 2010. http://www.mitsuba-renderer.org. 6

[LKYU12] LÖW J., KRONANDER J., YNNERMAN A., UNGER J.: BRDF models for accurate and efficient rendering of glossy surfaces. *ACM Trans. Graph. 31*, 1 (2012), 9:1–14. 2, 6, 7, 10

[MPBM03] MATUSIK W., PFISTER H., BRAND M., MCMILLAN L.: A data-driven reflectance model. *ACM Trans. Graph. 22*, 3 (2003), 759–769. 6, 7, 10

[NDM05] NGAN A., DURAND F., MATUSIK W.: Experimental analysis of BRDF models. In *Proc. Eurographics Symposium on Rendering* (2005), EGSR, pp. 117–226. 2, 7

[NRH*77] NICODEMUS F., RICHMOND J., HSIA J., GINSBERG W., LIMPERIS T.: Geometrical considerations and nomenclature for reflectance. *Applied Optics 9* (1977), 1474–1475. 2

[Per07] PERRON O.: Zur theorie der matrices. *Mathematische Annalen 64*, 2 (1907), 248–263. 4

[PM12] POLYANIN A. D., MANZHIROV A. V.: *Handbook of integral equations*. CRC Press, 2012. 4

[Rus98] RUSINKIEWICZ S. M.: A new change of variables for efficient BRDF representation. In *Rendering techniques '98*. Springer, 1998, pp. 11–22. 2

[Smi67] SMITH B.: Geometrical shadowing of a random rough surface. *IEEE Trans. Antennas and Propagation 15*, 5 (1967), 668–671. 2, 3

[TR75] TROWBRIDGE T. S., REITZ K. P.: Average irregularity representation of a rough surface for ray reflection. *J. Opt. Soc. Am. 65*, 5 (May 1975), 531–536. 8

[TS67] TORRANCE K. E., SPARROW E. M.: Theory for off-specular reflection from roughened surfaces. *J. Opt. Soc. Am. 57*, 9 (Sep 1967), 1105–1112. 2

[WMLT07] WALTER B., MARSCHNER S. R., LI H., TORRANCE K. E.: Microfacet models for refraction through rough surfaces. In *Proc. Eurographics Symposium on Rendering* (2007), EGSR, pp. 195–206. 2, 3, 6, 8, 9

[WZT*08] WANG J., ZHAO S., TONG X., SNYDER J., GUO B.: Modeling anisotropic surface reflectance with example-based microfacet synthesis. *ACM Trans. Graph. 27*, 3 (Aug. 2008), 41:1–9. 2, 7

[†] http://github.com/jdupuy/dj_brdf

Appendix A: Importance Sampling

We importance sample our microfacet BRDFs with the technique described by Walter et al. [WMLT07]. Our technique differs only in the sampling of the microfacet normal $\mathbf{h}$ from the tabulated data. To sample $\mathbf{h}$, we first produce slope variates $\tilde{\mathbf{h}} = (\tilde{x}_h, \tilde{y}_h)$ that are distributed according to P as follows. Let $P_1 \geq 0$ denote the marginal PDF $P_1(\tilde{x}_h) = \int_{\mathbb{R}} P(\tilde{x}_h, \tilde{y}_h)\, d\tilde{y}_h$. The PDFs P and P_1 are linked through the relation

$$P(\tilde{x}_h, \tilde{y}_h) = P_1(\tilde{x}_h)\, P_2(\tilde{y}_h|\tilde{x}_h) \Rightarrow P_2(\tilde{y}_h|\tilde{x}_h) = \frac{P(\tilde{x}_h, \tilde{y}_h)}{P_1(\tilde{x}_h)},$$

where $P_2 \geq 0$ is the PDF of $\tilde{y}_h$ conditioned on $\tilde{x}_h$. Let $F_1 \in [0,1]$ and $F_2 \in [0,1]$ respectively denote the cumulative distribution function of P_1 and P_2, i.e.,

$$F_1(\tilde{x}_h) = \int_{-\infty}^{\tilde{x}_h} P_1(\tilde{x})\, d\tilde{x},$$
$$F_2(\tilde{y}_h|\tilde{x}_h) = \int_{-\infty}^{\tilde{y}_h} P_2(\tilde{y}|\tilde{x}_h)\, d\tilde{y},$$

and $Q_1 = F_1^{-1}$ and $Q_2 = F_2^{-1}$ their respective quantile functions. Given realizations $u_1, u_2 \in [0,1]$ of two independent uniform variates, the variates obtained by the quantile transformation

$$\tilde{\mathbf{h}} = \begin{bmatrix} Q_1(u_1) \\ Q_2(u_2|Q_1(u_1)) \end{bmatrix}$$

are distributed according to P. We store Q_1 and Q_2 in a 1D and a 2D table, respectively. We compute the normal $\mathbf{h}$ from $\tilde{\mathbf{h}}$ with Equation (6).

Appendix B: Proof for the Isotropic Case

We show here how we arrived at Equation (22). We start from Equation (14) and apply Equation (21)

$$F_0\, g(\theta_o) = \int_{\Omega_+} K(\mathbf{o}, \mathbf{h})\, g(\theta_h)\, d\omega_h.$$

We then proceed with a few simple algebric manipulations, and Equation (22) naturally emerges

$$\begin{aligned} F_0\, g(\theta_o) &= \int_0^{2\pi} \int_0^{\pi/2} K(\mathbf{o}, \mathbf{h})\, g(\theta_h)\, \sin\theta_h\, d\theta_h d\phi_h \\ &= \int_0^{\pi/2} \left[\int_0^{2\pi} K(\mathbf{o}, \mathbf{h})\, \sin\theta_h\, d\phi_h \right] g(\theta_h) d\theta_h \\ &= \int_0^{\pi/2} K'(\theta_o, \theta_h)\, g(\theta_h)\, d\theta_h. \end{aligned}$$

Appendix C: Conversion to Analytic Roughness

Our slope distribution can be converted to anisotropic Beckmann or anisotropic GGX [Hei14] parameters straightforwardly. Both the Beckmann and GGX disributions depend on a scale matrix

$$\Sigma = \begin{bmatrix} \alpha_x^2 & \rho\alpha_x\alpha_y \\ \rho\alpha_x\alpha_y & \alpha_y^2 \end{bmatrix}.$$

We show next how to extract parameters $\alpha_x > 0$, $\alpha_y > 0$, and $\rho \in (-1, 1)$. Note that for isotropic PDFs, the extraction process may be simplified since we have $\alpha_x = \alpha_y$ and $\rho = 0$.

Beckmann The Beckmann microfacet slope PDF is

$$P_G(\tilde{\mathbf{h}}; \Sigma) = \frac{1}{\pi\sqrt{|\Sigma|}} \exp\left(-\tilde{\mathbf{h}}^t \Sigma^{-1} \tilde{\mathbf{h}}\right).$$

We retrieve the parameters of the scale matrix by computing 2nd order moments like in LEAN/LEADR mapping [DHI*13]

$$2\alpha_x^2 = \int_{\mathbb{R}^2} \tilde{x}_h^2\, P(\tilde{\mathbf{h}})\, d\tilde{\mathbf{h}}$$
$$2\alpha_y^2 = \int_{\mathbb{R}^2} \tilde{y}_h^2\, P(\tilde{\mathbf{h}})\, d\tilde{\mathbf{h}}$$
$$2\rho\alpha_x\alpha_y = \int_{\mathbb{R}^2} \tilde{x}_h \tilde{y}_h\, P(\tilde{\mathbf{h}})\, d\tilde{\mathbf{h}}.$$

Note that if $P = P_G$, then our conversion is exact.

GGX The GGX microfacet slope PDF is

$$P_X(\tilde{\mathbf{h}}; \Sigma) = \frac{1}{\pi\sqrt{|\Sigma|}} \left(1 + \tilde{\mathbf{h}}^t \Sigma^{-1} \tilde{\mathbf{h}}\right)^{-2}.$$

Note that the 2nd order moments diverge with GGX. We propose an alternative estimation to retrieve the parameters of the scale matrix

$$\alpha_x = \int_{\mathbb{R}^2} |\tilde{x}_h|\, P(\tilde{\mathbf{h}})\, d\tilde{\mathbf{h}}$$
$$\alpha_y = \int_{\mathbb{R}^2} |\tilde{y}_h|\, P(\tilde{\mathbf{h}})\, d\tilde{\mathbf{h}}$$
$$\beta_1 = \int_{\mathbb{R}^2} \frac{\tilde{x}_h \tilde{y}_h}{\tilde{x}_h^2 + \tilde{y}_h^2}\, P(\tilde{\mathbf{h}})\, d\tilde{\mathbf{h}}$$
$$\beta_2 = \int_{\mathbb{R}^2} \frac{\tilde{y}_h^2}{\tilde{x}_h^2 + \tilde{y}_h^2}\, P(\tilde{\mathbf{h}})\, d\tilde{\mathbf{h}}$$
$$\rho = \frac{\alpha_y}{\alpha_x} \frac{\beta_1}{\beta_1^2 + \beta_2^2}.$$

Note that if $P = P_X$, then our conversion is exact.

Figure 6: *Side-by-side fitting comparisons of a few isotropic materials from the MERL database [MPBM03].*

Figure 7: *Side-by-side fitting comparisons of a few anisotropic materials from the UTIA database [FV14].*